POSSIBLE DECREMENT OF LCO FLUTTER DYNAMIC PRESSURE DUE TO ROBUST CONTROLLER

Hiroshi Matsushita*, Takafumi Miyata, and Atsushi Fujimori*****
***University of Fukui, **Riken Sangyo, ***Shizuoka University**

Keywords: *transonic flutter, robust control, LCO, subcritical Hopf bifurcation*

Abstract

Bifurcation diagram of transonic flutter, either observed in the wind tunnel tests or predicted by the mathematical model, is classified as a subcritical Hopf bifurcation type, which means that the LCO type flutter may occur at lower dynamic pressure than the nominal flutter by more than 10 %. The present authors also developed the analytical method for the closed loop bifurcation diagram using a continuation method. Based on this method, the authors the possibility that the robust controller may bring about a larg decrement of LCO flutter dynamic pressure.

1 Introduction

In transonic regions, flutter often takes the form of a limit cycle oscillation (LCO) caused by the nonlinear behavior of the transonic aerodynamics due to a shock wave moving on the wing surface coupled with the flow separation. The present authors have developed a nonlinear mathematical model that can explain the most of the bifurcation characteristics observed in the series of transonic wind tunnel tests executed at the National Aerospace Laboratory (NAL, now the Japan Aerospace Exploration Agency) for a high aspect ratio wing model [1].

An efficient method to increase the flutter velocity in the transonic region may contribute greatly to aircraft performance improvement because in this region there is a phenomenon known as a transonic dip where the flutter velocity drops significantly against a flight Mach number. Active control technology of flutter is one of the most promising technologies that enable to increase the flutter velocity. The present authors proposed a practical control law design method that produces a robust controller against the model uncertainty [2].

Bifurcation diagram of transonic flutter, either observed in the wind tunnel tests or predicted by the mathematical model, is classified as a subcritical Hopf bifurcation type, which means that the LCO type flutter may occur at lower dynamic pressure than the nominal flutter, by more than 10 %. The present authors also developed the analytical method for the closed loop bifurcation characteristics using a continuation method [3]. Making use of these methods, the authors discusses in this paper the possibility of decrease in LCO flutter dynamic pressure caused by control, in particular, by a robust controller.

2 Nonlinear Mathematical Model for Transonic Flutter

2.1 Experimental Observation of Bifurcation in Transonic Flutter

Figure 1 shows a wind tunnel model of a high aspect ratio wing. It has a leading edge- and a trailing edge-control surface (shown as hatching parts). They are used for active flutter control research [4]. The wing has an inflated middle part where two sets of electric motors for control are installed. For LCO investigation in the wind tunnel tests, a leading edge control surface is used as a source of excitation and wing response is measured by four accelerometers and seven sets of torsion and bending strain gages, which are fixed along an aluminum spar of the wing.

In the series of wind tunnel experiments at the transonic wind tunnel of NAL, it was turned out that this wing behaves a typical transonic flutter. The wing has a minimum dynamic pressure at a transonic region (transonic dip) and every flutter has the form of LCO. In each flutter, when the tunnel pressure is increased as shown at the bottom time chart in Fig. 2 as a typical case of Mach 0.8, the wing jumps up to LCO at a specified (nominal) dynamic pressure as shown at the top chart in the figure. (Since this figure shows the active flutter test result [4], the LCO flutter is stopped right after its occurrence by activating a trailing edge control surface as shown at the middle chart.) Successive investigation cleared that, even at lower dynamic pressure than the nominal pressure stated above, the wing can be brought into LCO state if it's excited above a certain energy level. Once LCO state is attained, it is kept continuing even after removing the excitation. LCO thus attained is stabilized again if the tunnel pressure is further decreased. These phenomena are presented in Fig. 3 where the LCO is established by a leading edge excitation as shown at the middle chart in this case, and continues to oscillate even after removing the excitation. Then LCO continues to oscillate during the quasi-steady decrease of the wind tunnel pressure until it ceases to rest at a certain value of the pressure. That point corresponds to a saddle-node bifurcation.

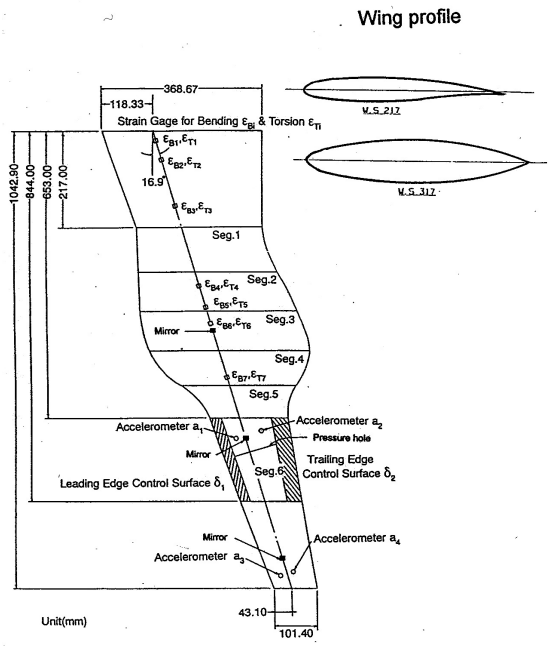

Fig. 1 High aspect ratio wing model

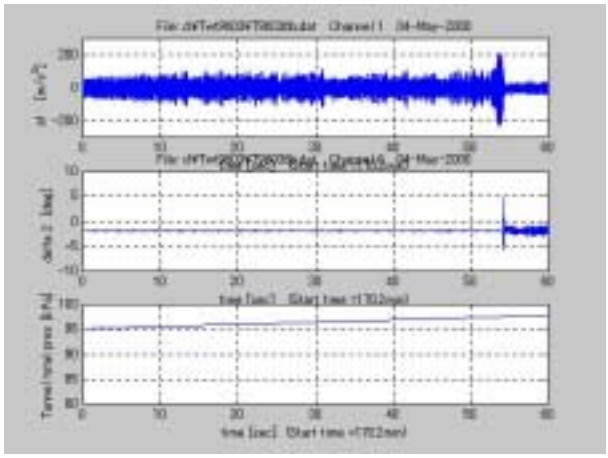

Fig. 2 Time history of nominal flutter occurrence during the increase of the wind tunnel pressure.

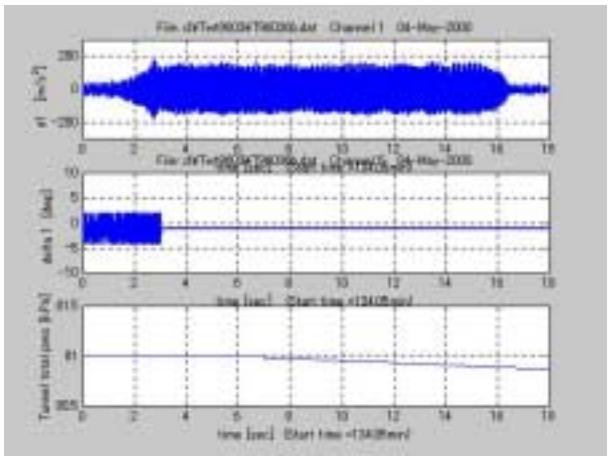

Fig. 3 Quasi-steady decrease of the dynamic pressure at the saddle-node bifurcation

Figure 4 summarizes these phenomena found in the tests as a bifurcation diagram

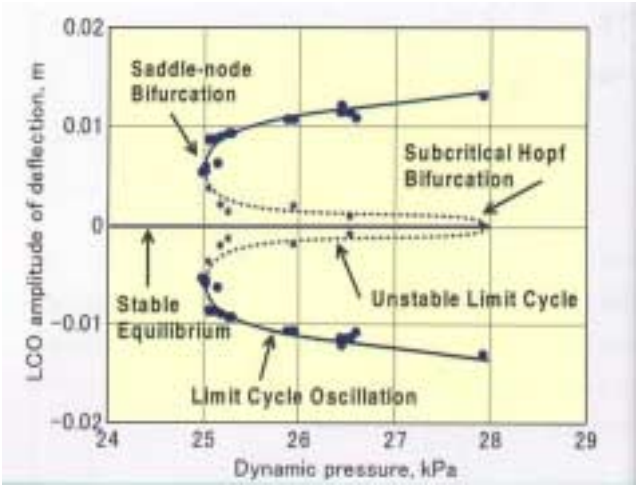

Fig. 4 Bifurcation diagram obtained

where the LCO amplitude is depicted against the dynamic pressure. In this figure the stability boundary, or unstable limit cycle expressed by the crosses, has a deviation and the stable region under the boundary is rather narrow. Disturbances around the wing such as turbulence in the wind tunnel flow, the flow separation occurred at the wing surface, etc., may decrease the stable region in the experimentally obtained diagram.

2.2 Nonlinear Mathematical Modelling

The first author *et al*. have developed a nonlinear mathematical model in the form of 2-DOF, finite state nonlinear differential equation [6]. Introducing the fourth order nonlinearity to the generalized aerodynamic damping terms, they have obtained the following sixth order nonlinear differential equation,

$$\dot{x} = Ax + \Delta A_{NL}x + Bu; \quad x = [q,\ \dot{q},\ z]^T \in R^6 \qquad (1)$$

where q is the generalized coordinates and z is the augmented variable expressing the unsteady aerodynamic delay. The matrix A is a linear part of the system matrix and is an ordinary matrix for flutter analysis. It takes a form as,

$$A=\{a_{ij}\}=\begin{bmatrix} 0 & I & 0 \\ -(M-A_0)^{-1}(K-A_2) & -(M-A_0)^{-1}(C-A_1) & -(M-A_0)^{-1} \\ B_a & 0 & -\Lambda \end{bmatrix} \in R^{6\times 6} \qquad (2a)$$

and

$$B = \begin{bmatrix} 0 \\ -M_q S_\delta K_\delta \\ K_\delta \\ 0 \end{bmatrix} \in R^{14\times 1} \qquad (2b)$$

In eq. (4), M, C, and K are mass, structural damping, and stiffness matrices, respectively, used in the following fundamental aeroelastic equation of a flexible wing.

$$M\ddot{q} + C\dot{q} + Kq = f_a \qquad (3)$$

The aerodynamic term f_a in right hand side is approximated by the finite state form:

$$f_a = A_2\ddot{q} + A_1\dot{q} + A_0 q + z \qquad (4)$$
$$z = \Lambda z + B_0 q$$

where $\Lambda = diag(-\lambda,\cdots,-\lambda)$.

The matrix ΔA_{NL} in eq. (1) represents a nonlinear terms and has the following form.

$$\Delta A_{NL}=\begin{bmatrix} 0 & 0 & 0 \\ 0 & (M-A_0)^{-1}\Delta A_{1NL} & 0 \\ 0 & 0 & 0 \end{bmatrix} \in R^{6\times 6} \qquad (5)$$

where the diagonal components of the aerodynamic damping part $(M-A_0)^{-1}\Delta A_{1NL}$ has the fourth order nonlinear terms such as

$$\Delta A_{1NL} = \begin{bmatrix} (\beta_1 q_1^{\ 2} + \gamma_1 q_1^{\ 4})a_{11a} & 0 \\ 0 & (\beta_2 q_2^{\ 2} + \gamma_2 q_2^{\ 4})a_{22a} \end{bmatrix} \qquad (6)$$

where a_{11a} and a_{22a} are the aerodynamic damping coefficients for torsion and bending deflection, respectively. The parameters β's and γ's are free parameters to be determined for fitting the wind tunnel test data. When the parameters β's and γ's are set to be zero, the equation (1) is reduced to an ordinary linear flutter equation.

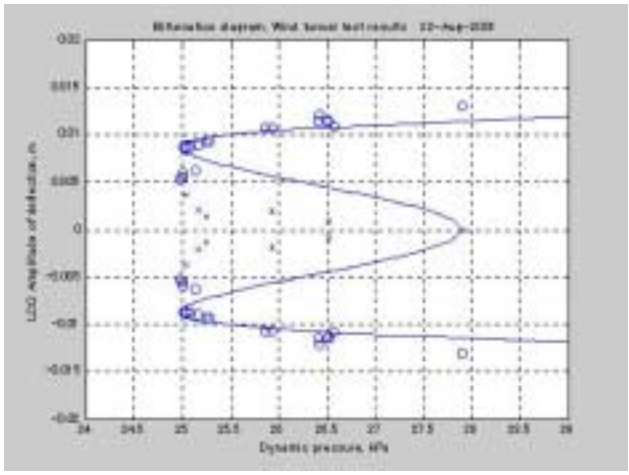

Fig. 5 Bifurcation diagram of the math model with optimized parameters and the experimental results.

Making a lots of efforts to search an optimum combination of parameters, we have reached the values of β = -6.5e-3 and γ = 2.5e-5. Resulting bifurcation diagram is shown as a solid line in Fig. 5. In the figure experimental data are also plotted. The correspondence of the LCO between the math model and the experiment is quite good; the amplitude of LCO is almost identical and the position of the saddle-node bifurcation is exactly the same. There still remains a difference in unstable limit cycle; the

mathematical model has a wide stable area under the unstable limit cycle, while the experimental data shows a limited region of stability. As stated earlier, the main reason of this discrepancy may exist in the noise effects. In real situation, even at the stable region disturbance may energize the wing to jump up to unstable region and push the wing to LCO state.

Besides the state equation (1), the output equation is necessary to design the flutter control system since the states in the Eq. (1) comprises of the generalized coordinates which cannot be observed directly. When the acceleration is used as an output, the output equation takes the form as follows,

$$y = Cx + Du + v(t) \tag{7}$$

where the coefficient matrices are

$$\boldsymbol{C} = \left[\left(\mathbf{Z}_q \mathbf{A}_1 - g \frac{\partial \mathbf{Z}_q}{\partial y} \right) \quad \mathbf{Z}_q \mathbf{A}_2 \quad \mathbf{Z}_q \mathbf{A}_3 \quad \mathbf{Z}_q \mathbf{A}_4 \quad \mathbf{Z}_q \mathbf{A}_5 \right] \in R^{1\times 14} \tag{8a}$$

$$D = -Z_q M_q S_\delta K_\delta \in R^{1\times 1} \tag{8b}$$

3 Control Law Design for Flutter Suppression and Closed Loop Bifurcation Diagram

3.1 LQG Controller Design

To this multi-input and multi-output plant, the LQG synthesis method can be applied to obtain the optimal full state/full order feedback control laws. For flutter control, the performance index can be defined by the system mechanical energy plus control cost as follows,

$$J = \int \left\{ \frac{1}{2} x^T(t) Q x(t) + \frac{1}{2} R u(t)^2 \right\} dt \tag{9}$$

Since the state equation, the output equation and the performance index are provided in the standard form of the optimal output regulator problem, the full-order output feedback control law can be derived as a combination of a regulator and Kalman estimator as follows [7]. First, the state feedback optimal regulator part can be expressed using an estimated state as,

$$u = -K_1 \hat{x} \tag{10}$$

where the optimal gain K_1 is given as,

$$K_1 = R^{-1} B^T P_1 \tag{11}$$

and P_1 is the solution to the following matrix Riccati equation.

$$A^T P_1 + P_1 A - P_1 B R^{-1} B^T P_1 + Q = 0 \tag{12}$$

As a state observer, the present synthesis method utilizes Kalman estimator; the dynamics of the estimator have the following formula.

$$\dot{\hat{x}} = A\hat{x} + Bu + K_2 \left(y - C\hat{x} - Du \right) \tag{13}$$

where the Kalman gain K_2 is given by the other Riccati equation such as,

$$AP_2 + P_2 A^T - P_2 C^T V^{-1} C P_2 + W = 0 \tag{14}$$

$$K_2 = P_2 C^T V^{-1} \tag{15}$$

The order of this output feedback controller is the same as the plant. Since a full order controller has in general too high an order to be implemented in an on-board computer in read time sense, order reduction is necessary. Furthermore, there might be some state variables in the control law that makes a lesser contribution to the control performance. Using the order reduction method of a residualization and a balanced truncation approximation, we can finally obtain the following form of reduced order output feedback control law.

$$\dot{z} = Fz + Gy \tag{16a}$$

$$u = Hz \tag{16b}$$

3.2 Bifurcation Analysis for a Closed Loop System

In this section the procedure of bifurcation analysis for a closed loop system is developed using a continuation method. The homogeneous equation is derived from the open loop equation with a control law. Substituting the control law, eq. (13) into the state equation (1) with the out-

put equation (7), we can obtain the following homogeneous equation for closed loop system,

$$\begin{bmatrix} \dot{x}(t) \\ \dot{\hat{x}}(t) \end{bmatrix} = \tilde{Ao} \begin{bmatrix} x(t) \\ \hat{x}(t) \end{bmatrix} \qquad (17)$$

The system coefficient is

$$\tilde{Ao} = \begin{bmatrix} A(D_p) + \Delta A_{NL}(D_p) & -B(D_p)K_1 \\ K_2 C(D_{pd}) & A_F(D_{pd}) \end{bmatrix} \in R^{28\times} \qquad (18)$$

where $A_F(D_{pd}) = A(D_{pd}) - B(D_{pd})K_1 - K_2 C(D_{pd})$ should be noticed as constant. Even though the dimension of the system has increased to double, a continuation method can be applied as an open loop system since the equation is the same form as a homogeneous one. Figure 6 shows the results of the analysis obtained for the case of LQG controller. In this figure an open loop bifurcation is depicted as well in thin solid line,

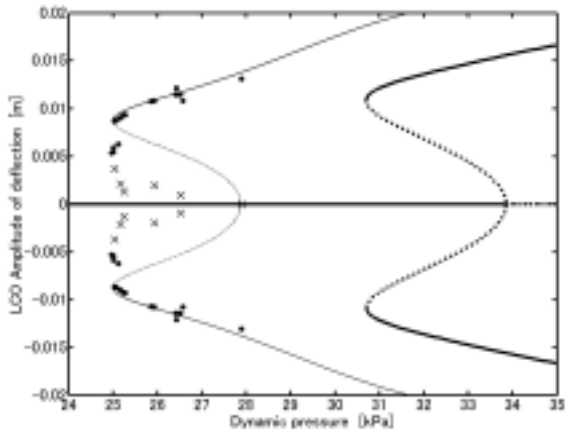

Fig. 6 Bifurcation diagram of the closed loop system with LQG controller

while the closed loop bifurcation is in thick solid line. In designing the LQG controller, the design dynamic pressure is set at 30.9 kPa, and the weight for control is selected as 5000.

Figure shows that the closed loop system comprosed of the nonlinear system and a linear control law can be analyzed by a continuation method as well as an open loop system. The closed loop bifurcation diagram is almost shifted to the right and the open loop dynamic pressure of 27.9 kPa can be increased to 33.4 kPa implying 19.7% improvement.

3.3 Robust Controller Design

3.3.1 Design Procedure

Robust stabilization method was applied to manage a mathematical model insufficiency. The design specification was determined to extend the open loop flutter dynamic pressure at Mach 0.8 by 10.7% within an allowable control surface activation of 1 deg deflection and 90 deg/sec angular velocity. Furthermore, in case of robust design, the specification should be satisfied against 10% deviation of aeroelastic parameters of the first and the second mode stiffness which have the critical effect to plant stability.

Robust stability control design based on left coprime factors approach was applied to this wing model and the reduced order controller was obtained by the residualization method yielded control laws with a certain level of robustness [4]. The design process combines classical open-loop shaping principle with an robust stabilization problem in the normalized coprime factors framework [7]. Main contents of the procedure are summarized here.

Let the nominal plant model $P(s)$ has a normalized left coprime factorisation such as,

$$P(s) = M(s)^{-1} N(s) \qquad (19)$$

where

$$M(s)M(-s)^T + N(s)N(-s)^T = I \qquad (20)$$

for all s, and $M(s), N(s) \in RH_\infty$ are asymptotically stable proper real rational functions. The uncertainties in the plant can be represented in terms of additive stable perturbations Δ_M, Δ_N to the factors in a coprime factorization of the plant. Then representing the plant $\tilde{P}(s)$ as,

$$\tilde{P} = (M + \Delta_M)^{-1}(N + \Delta_N) \qquad (21)$$

$$D_\varepsilon \equiv \{\Delta = (\Delta_N, \Delta_M) \mid \Delta \in RH_\infty, \|\Delta\|_\infty < \varepsilon\} \qquad (22)$$

the sufficient condition of the controller that can stabilize the perturbed is given as

$$\left\| \begin{bmatrix} K_I \\ I \end{bmatrix} (I - PK_I)^{-1} M^{-1} \right\|_\infty \le \varepsilon^{-1} \qquad (23)$$

Let a minimal realization of a proper plant be $P(s) = (A, B, C, D)$, and X, Y be the positive definite solutions of the following algebraic Riccati solutions,

$$A_a{}^T X + XA_a - XB_a B_a{}^T X + C_a{}^T C_a = 0 \qquad (24)$$

$$A_a Y + YA_a{}^T - YC_a{}^T C_a Y + B_a B_a{}^T = 0 \qquad (25)$$

and the maximum value of a stability margin $\varepsilon_{\max}$ given by the following equation,

$$\varepsilon_{\max} = (1 + \lambda_{\max}(XY))^{-1/2} \qquad (26)$$

where $\lambda_{\max}(XY)$ is a Hankel norm, i. e., a maximum eigenvalue of the product of the positive definite solutions, X, Y. Choosing the stability margin ε such that $0 < \varepsilon < \varepsilon_{\max}$, then, the state space realization of a central controller $K_I(s)$ can explicitly be given, using Doyle's notation, as

$$K_I = \begin{bmatrix} \boldsymbol{A_a} - \boldsymbol{B_a B_a}^T \boldsymbol{X} + \varepsilon^{-2} \boldsymbol{W_r}^{-T} \boldsymbol{Y C_a}^T \boldsymbol{C_a} & \varepsilon^{-2} \boldsymbol{W_r}^{-T} \boldsymbol{Y C_a}^T \\ \boldsymbol{B_a}^T \boldsymbol{X} & 0 \end{bmatrix} \qquad (27)$$

$$W_r = (1 - \varepsilon^{-2})I + XY \qquad (28)$$

In order to incorporate performance objectives in the design process, input and output shaping functions $W_i(s)$, $W_o(s)$ are introduced just before and after the normal plant. The extended plant is thus given as $G_e(s) = W_o(s)P(s)W_i(s)$ so that feedback controller can be given as

$$K_e(s) + W_i(s)K_I(s)W_o(s) \qquad (29)$$

where a controller $K_I(s)$ is obtained from Eq. (16) by substituting a plant dynamics $P(s)$ with $P_e(s) = (A_e, B_e, C_e, D_e)$. The maximum stability margin for an extended plant can be expressed accordingly as

$$\varepsilon_{e\max} = (1 + \lambda_{\max}(X_e Y_e))^{-1/2} \qquad (30)$$

3.3.2 Robust Controller Design

Robust controller was designed first by setting an output shaping filter as a constant as $W_o = 1$, 2, 3, 5 resulting a performance of a full order controller as shown in Table 1.

Table 1 Full-order controller performances

W_o	$\varepsilon_{\max}$	δ_{rms} [deg]	$\dot{\delta}_{rms}$ [deg/s]
1	0.3786	0.2408	50.46
2	0.3929	0.3222	78.01
3	0.3788	0.3991	105.5
5	0.3401	0.5282	159.6

According to the design criteria of control surface activation of 1 deg deflection and 90 deg/sec angular velocity, we decided to choose $W_o = 2$.

Preventing an excessive control surface movement at a higher frequency, we placed a

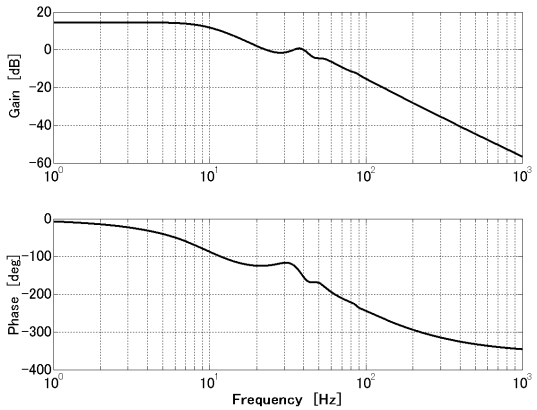

Fig. 7 Bode diagram of the final controller

first order low pass filter as a compensator as

$$W_o(s) = \frac{2}{(2\pi \times 20)s + 1} \qquad (31)$$

Furthermore, applying a notch filter in order to preventing a coupling to the third mode with the controller, we finally obtained the compensator ,

$$W_o(s) = \frac{2(s^2 + 0.5*(2\pi \times 48)s + (2\pi \times 48)^2)}{(\frac{s}{(2\pi \times 20)} + 1)(s^2 + (2\pi \times 48)s + (2\pi \times 48)^2)} \qquad (32)$$

Figure 7 shows the Bode diagram of this controller where the design parameters are: $\varepsilon_{\max}$ = 0.3443, δ_{rms}=0.2384deg, and $\dot{\delta}_{rms}$= 36.72deg/s. The stability margin therefore is ε = 0.95× $\varepsilon_{\max}$ = 0.327 and the order of the controller results in 22.

The Bode diagram of the controller that was used in the transonic wind tunnel testing carried out at NAL and attained 10.9% increase of flutter speed [4] is shown for comparison in Fig. 8. The controller is reduced to the order of eight. Comparing both figures we can see that the controller gains are almost at the same level and the newly designed controller would not enforce any excessive deflection to the control surface, which might prevent the control system locked.

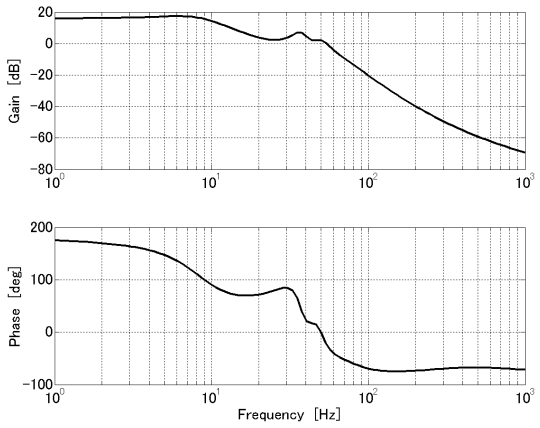

Fig. 8 Bode diagram of the controller used in wind tunnel test

3.3.3 Bifurcation Diagram for Robust Controller

Applying the same procedure as the LQG controller, we can depict the closed loop bifurcation diagram for the robust controller thus designed. For the robust controller, the total order has increased as much as 38th order. In figure 9 the bifurcation diagrams are compared for an open loop system (I), LQG controller (II) and a robust controller (III). In this particular numerical setup of the design parameters, the robust controller attained the higher increase of flutter dynamic pressure than the LQG controller.

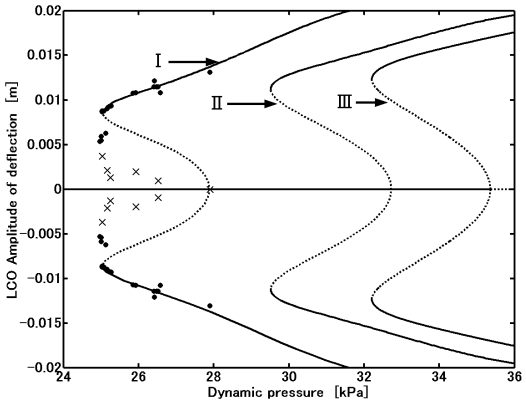

Fig. 9 Bifurcation diagram of the closed loop system with robust controller

4 Possible Decrease of Flutter Dynamic Pressure due to Control

In designing the control law, the nominal closed loop flutter dynamic pressure can be increased if the design dynamic pressure is set at higher value. However, the problem may occur that the saddle-node bifurcation point will not be increased so much as the nominal point and the stability boundary will also be decreasing as shown in Fig. 10.

In Fig. 10 the design dynamic pressures are increased from the left to the right as 30.9, 33.1,

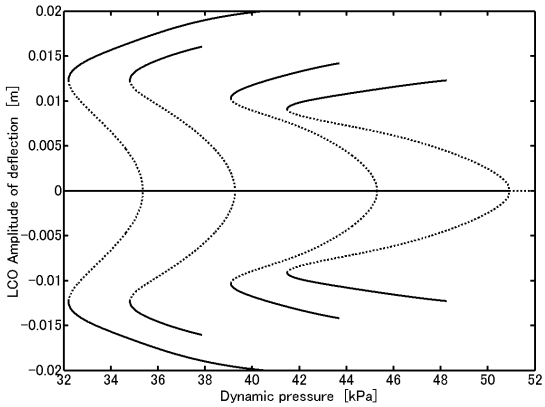

Fig. 10 Bifurcation diagram of each designed point (robust control)

34.3, 35.5 kPa, respectively. In case of LQG controller, the trend of saddle-node bifurcation is similar to the robust controller, but the posi-

tion of the stability boundary is not so much changed as in the robust controller as shown in Fig. 11. In this figure, the design dynamic pressures are changing in the same way as the robust controller.

We tried to analyze the bifurcation diagram for the control law that used in the previous wind tunnel tests as described in the section 3.3.2 [4]. Figure 12 shows the results of analysis, which shows that even though the nominal flutter dynamic pressure can be increased, the saddle-node point is not increased anymore. Though the saddle-node bifurcation has not been verified in the wind tunnel tests, this figure make caution about the possibility of great reduction of the effect of the control in saddle-node point and the stability boundary.

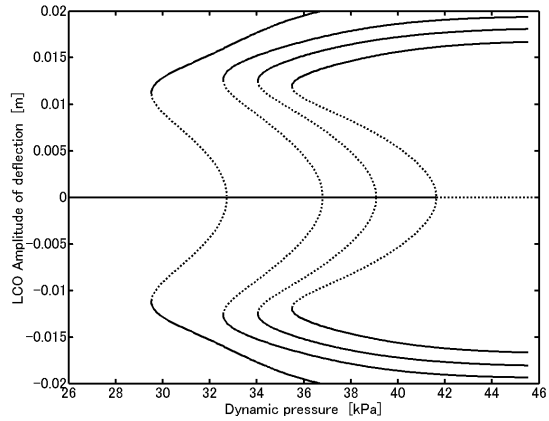

Fig. 11 Bifurcation diagram of each designed point (LQG control)

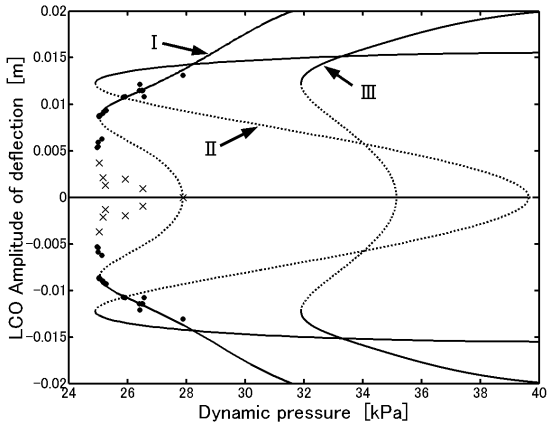

Fig. 12 Bifurcation diagram of the closed loop system with robust controller

5 Conclusions

The analytical method of the closed loop bifurcation diagram for the nonlinear system with a linear controller is developed using a continuation method. When the robust controller is applied, it's possible that the stability margin will not increase so much as a nominal flutter dynamic pressure in that a dynamic pressure of a saddle-node point is almost the same as for an open loop system. Even if the dynamic pressure can be increased by a certain amount, the LCO flutter may occur at a low dynamic pressure of no significant increase to an open loop LCO flutter.

References

[1] Matsushita, H., Miyata, T., Christiansen, L. E. Lehn-Schiøler, T. and Mosekilde, E. "On the Nonlinear Dynamics Approach of Modeling the Bifurcation for Transonic Limit Cycle Flutter," *Proceedings of the 23rd International Congress of the Aeronautical Sciences*, pp. 414.1 - 414.8, 2002.

[2] Fujimori, A., Matsushita, H., and Saitoh, K., "Model Modification of Transonic Aerodynamic Force on a High Aspect Ratio Aeroelastic Wing and Its Active Flutter Supression," *Proceedings of the 23rd International Congress of the Aeronautical Sciences, Harrogate,* 2000.

[3] Miyata, T. and Matsushita, H., "Nonlinear Mathematical Modeling of Aircraft Flutter and Its Closed Loop Bifurcation Characteristics," Proceedings of SICE Annual Conference 2003 in Fukui, 2003.

[4] Saitoh, K. Baldelli, D. H. Matsushita, H., and Hashidate, M. Robust controller design and its experimental validation for active transonic flutter suppression. *Proceedings of CEAS International Forum on Aeroelasticity and Structural Dynamics 1997*, Vol. II, Rome, 1997, pp. 393-399.

[5] Matsushita, H., Saitoh, K., and Gránásy P. Two degrees-of-freedom nonlinear math model with fourth order nonlinear aerodynamics for transonic limit cycle flutter. *CEAS/AIAA/ICASE/NASA LaRC International Forum on Aeroelasticity and Structural Dynamics 1999*, Williamsburg, US, June 1999.

[6] Kwakernaak, H. and Sivan, R., "*Linear Optimal Control Systems*," Whiley-Interscience, 1972.

[7] Mcfarlen, D. C. and Glover, K., "*Robust Controller Design Using Normalized Coprime Factor Plant Descriptions*, " Springer-Verlag, 1990